

Diffraction based single pulse measurement of air ionization dynamics induced by femtosecond laser

LIN ZHANG,¹ JIAMIN LIU,¹ WENQI GONG,¹ HAO JIANG,^{1,2}  AND SHIYUAN LIU^{1,3} 

¹State Key Laboratory of Digital Manufacturing Equipment and Technology, Huazhong University of Science and Technology, Wuhan 430074, China

²hjiang@hust.edu.cn

³shyliu@hust.edu.cn

Abstract: A single pulse diffraction method to probe the plasma column evolution of the air ionization induced by the femtosecond laser pulse has been proposed. By utilizing a linearly chirped pulse as the probe light, the spatiotemporal evolution spectrum of the plasma column can be acquired in a single measurement. A method based on the Fresnel diffraction integral is proposed to extract the evolution of the phase shift after the probe light is crossing through the plasma column. Results show that the plasma expands rapidly within 7 ps due to the ionization, and then reaches a steady state with a diameter of about 80 μm with the pump pulse energy of 1 mJ. Furtherly, the temporal profile of the free electron density and the refractive index in the plasma region were determined using the corresponding physical models. The single-shot method can be expected to broaden the way for detecting the dynamics of the femtosecond laser-induced plasma.

© 2021 Optical Society of America under the terms of the [OSA Open Access Publishing Agreement](#)

1. Introduction

Air ionization and plasma induced by the ultrafast laser have attracted a lot of attention and research interests in the last twenty years [1, 2]. When the femtosecond laser is focused in the air, the molecules in the air absorb photon energy and are ionized in the form of multiphoton ionization and avalanche ionization. As a result, a large amount of hot plasma is formed in the focal area, which expands to the surroundings and generates shock waves [3–5]. The extreme conditions of plasma (ultra-high electron density and temperature, etc.) make it widely used in the fields of remote sensing [6], laser-guided discharges and lightning control [7–9], and ignition systems [10]. Therefore, an accurate understanding of the evolution of the plasma and its parameters is the prerequisite for exerting its potential in industrial applications and fundamental research. In order to understand the properties of the plasma column left by the femtosecond pulse, the characterization of the size and electron density of the plasma is very important.

Plasma generated by femtosecond laser could be light filaments or plasma column and has variable size [11–13], which is very dependent on the external focusing conditions [14]. Regarding the determination of the electron density, different methods have been reported. Such as the electric conductivity method [15–17], the interferometric method [12, 18–21] and the plasma diffraction method [11, 16, 22–25]. Interferometry and the diffractometry based methods measure the plasma parameters by analyzing the phase shift of the probe light after passing through the plasma column. However, in order to acquire the temporal evolution of the plasma with multiple pulses, it is necessary to adjust the delay line for many times in the experimental configuration and the temporal resolution depends on the minimum differences among these delays. Considering the changes between pulses and fluctuations in the test environment may introduce system errors, single-shot based method is of great importance for quantitative analysis for such ultra-fast

processes. In 2000, C. Y. Chien *et al.* combined interferometry with chirped pulses to measure the ionization dynamics of air driven by the femtosecond laser [26]. Similarly, the single-shot supercontinuum spectral interferometry (SSSI) has been proposed to detect the ionization of helium [27] and the transient nonlinear refractive index in gases [28]. However, interferometry requires precise control of the pulses timing to ensure the reference pulse precedes the pump pulse, meanwhile the probe pulse overlapped with the pump pulse in time. In 2005, J. Liu *et al.* theoretically proposed a linearly chirped longitudinal diffractometry based method to investigate the plasma dynamics [22], in which this longitudinal method assumes that the plasma density is evenly distributed along the axis of the plasma column. The single-shot measurement method of the femtosecond laser-induced plasma dynamic evolution still needs to be further expanded.

In this paper, a single pulse diffraction method based on the pump-probe technology was proposed to measure the dynamic process of air ionization from the transverse direction, with which the electron density distribution along the length of the plasma column is not necessary to be considered. The spatiotemporal spectrum of the plasma column evolution can be obtained in a single measurement by utilizing the linear chirped pulse. From the spectrum, we can directly obtain the evolution of air ionization, including the formation, expansion and stabilization of the plasma column. The result shows that the plasma expansion lasted about 7 ps and the diameter of the stable plasma column was about 80 μm with the pump pulse energy of 1 mJ. Furtherly, a method based on the Fresnel diffraction integral has been developed to extract the phase shift temporal profile of the probe light. Through the relationship between the phase shift and the electron density, the temporal evolution of the electron density and the refractive index in the plasma region is acquired.

2. Experiment configuration and method

2.1. Experiment scheme

The schematic diagram of the proposed single pulse method for detecting the air ionization process is shown in Fig. 1 (a). A Ti: sapphire laser (Newport Corporation, SOL-ACE35F1K-HP) is used to deliver 35 fs Gaussian limit pulses with central wavelength of 800 nm and the maximum single pulse energy of ~ 7 mJ. The repetition rates of the output pulse of the system can be adjusted in integer multiples from 1 Hz to 1 kHz, and 10 Hz was used in this work. In the light path, the output femtosecond pulse is split into two beams by a non-polarizer beam splitter. The beam with 80% pulse energy is going to excite air ionization through a focusing lens (LA1951-B, THORLABS) with focal length of 25.4 mm and diameter of 25.4 mm. The single pump pulse used in the experiment is 1 mJ, which is measured by a power meter. The peak power density can reach $\sim 10^{17}$ W/cm² in the focal area. A mechanical shutter (SH1/M, THORLABS) with open time of 0.1 s was used to ensure that only one pulse was focused in a single measurement. Meanwhile, the beam with 20% pulse energy enters a home-made grating-based pulse stretcher, which converts the fs pulse into a linear chirped pulse. The linear relationship between the wavelength and time of the stretched pulse can be expressed as $\lambda = 0.1124 \cdot t + 786.2$, where 0.1124 is the linear coefficient with unit of nm/ps. The details of the pulse stretcher and the chirp parameters measurement can be found in our previous work [29]. The chirped pulse transits a polarizer to generate a *p*-polarized light. A neutral filter wheel with a variable filter ratio is used in the probe path to protect the detector. A delay line is used to ensure the simultaneity of the probe light and the pump light. An achromatic lens (ACA254-075-B, THORLABS) with focal length of 75 mm is employed to focus the probe beam, result in a spot size about 500 μm at the detection point, which completely covers the diameter of the plasma column, as shown in Fig. 1(b). Through another achromatic lens (ACA254-050-B, THORLABS) with focal length of 50 mm, the plasma column is imaged onto the slit of an imaging spectrometer (Horiba, iHR550), as shown in Fig. 1(c). Finally, a diffraction fringe spectrum will be recorded on the CCD detector (Horiba, Syncer-1024 \times 256). According to the previous measured chirped coefficient and the

spectral range (~ 31.7 nm) of the CCD detector, the corresponding measurement range is about 282 ps in a single pulse shot.

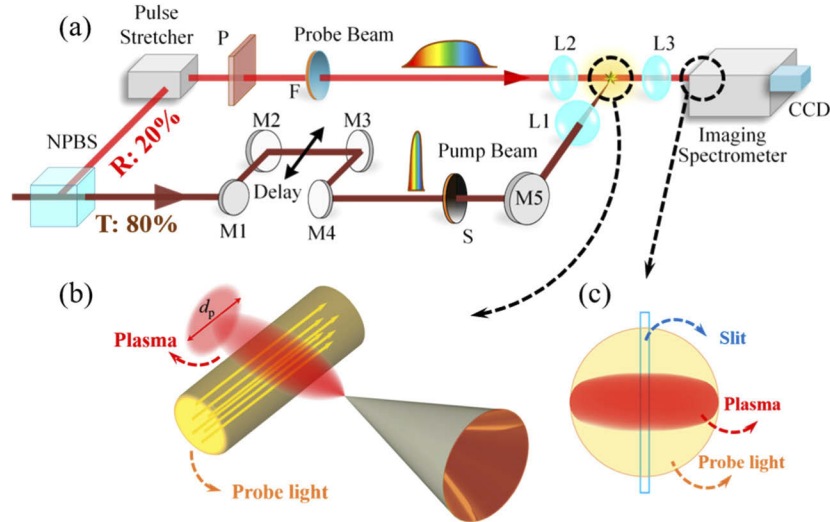


Fig. 1. (a) The schematic diagram of the pump-probe based optical configuration. (b) the formed plasma column and the probe light. (c) the region that entered the imaging spectrometer through the slit of the spectrometer with a normal angle view. The probe beam is a linear chirped pulse. NPBS: non-polarized beam splitter; P: polarizer; F: neutral filter wheel; M: mirror; S: mechanical shutter; L: lens.

2.2. Method for dynamic parameter extraction

When the femtosecond laser pulse is focused in the air, the gas molecules will be ionized and forming plasma column in the focal region due to the ultra-high energy density. When the probe pulse passes through the plasma region, diffraction fringe will be formed in the detector due to the phase shift induced by the large amount of plasma. Based on the diffraction principle, a spatial-spectral diffraction spectrum can be obtained in a single measurement by the described equipment, which contains the dynamic information of the plasma evolution. The radial size of the plasma generated by ionization and the phase shift of the probe light can be obtained by fitting the diffraction fringe based on the Fraunhofer and Fresnel diffraction. An important premise of the fitting process is that the plasma is uniformly distributed in the radial direction of the ionization region. Another prerequisite is that the vertical distribution of the phase shift is not considered in this work. Accordingly, the resulted phase shift $\Delta\varphi$ is invariant in the radial space within the plasma, and $\Delta\varphi = 0$ when exceeding the radius of the plasma region. The probe light in this work has a Gaussian profile defined as,

$$E_0(r) = \exp(-ar^2) \times \exp(-j\Delta\varphi), \quad (1)$$

where r represents the radial direction. The simplified form of the Fresnel diffraction integral formula used to fit the diffraction fringe can be expressed as follows, which consists of a Gaussian function, a Bessel function and a Cosine function [11, 22],

$$I(r) = -\text{sgn}(M)C\pi r_p^2 \frac{1}{\sqrt{a^2 + M^2}} \exp(-B_1 r^2) - \frac{J_1(2Mr_p r)}{2Mr_p r} \times \cos\left(B_2 r^2 - \frac{\Delta\varphi}{2}\right) \sin\left(\frac{\Delta\varphi}{2}\right), \quad (2)$$

where $I(r)$ is the difference of the electric field intensity with and without plasma generation, $\text{sgn}(M)$ is the sign of M and $M = \pi/\lambda d$, where d is the distance between the plasma column and

the CCD camera, λ is the wavelength of the probe light. C is a constant, r_p is the mean radius of the plasma column. $B_1 = M^2 a / (a^2 + M^2)$, $B_2 = M^3 / (a^2 + M^2)$, J_1 represents the first order Bessel function. The diffraction fringes obtained in this work are equivalent to the fringes extracted from the diffraction pattern in [11]. Therefore, Eq. (2) can be used to solve the phase shift of the probe light.

The radius of the plasma column and the phase shift at a certain moment can be acquired using Eq. (2). However, the dynamic changes of the plasma within the entire measurement range in a single shot cannot be obtained through a single fitting process. In order to extract the phase shift evolution from the measured spectrum, we assumed that the change in the plasma column radius is negligible when the plasma approaches its steady state. Based on this approximation, the time-varying phase shift $\Delta\varphi$ is the only parameter to be solved in Eq. (2). Therefore, the dynamic change of $\Delta\varphi$ can be solved by extracting the temporal evolution of spectral intensity at any spatial location (this work takes the case of $r = 0$). The corresponding expression can be written as,

$$\Delta\varphi(\omega) = \arcsin \left(\frac{2I_{\text{meas}}(\omega, 0)}{I_1|_{r=0}I_2|_{r=0}} \right), \tag{3}$$

where $I_{\text{meas}}(\omega, 0)$ represents the measured spectral intensity change. $I_1 = -\text{sgn}(M)C\pi r_p^2(a^2 + M^2)^{-1/2}\exp(-B_1 r^2)$ and $I_2 = J_1(2Mr_p r)/2Mr_p r$ represent the Gaussian function part and the Bessel function part of Eq. (2), respectively. The result $\Delta\varphi(\omega)$ calculated by Eq. (3) can be converted to the temporal profile $\Delta\varphi(t)$ through the aforementioned time-frequency mapping relationship of the chirped pulse. The whole calculation process of the developed method to extract the phase shift evolution is summarized as shown in Fig. 2. It should be noted that, the phase shift obtained using the experimental configuration in this work (the probe is perpendicular to the pump) is the phase shift of a cross section of the plasma column.

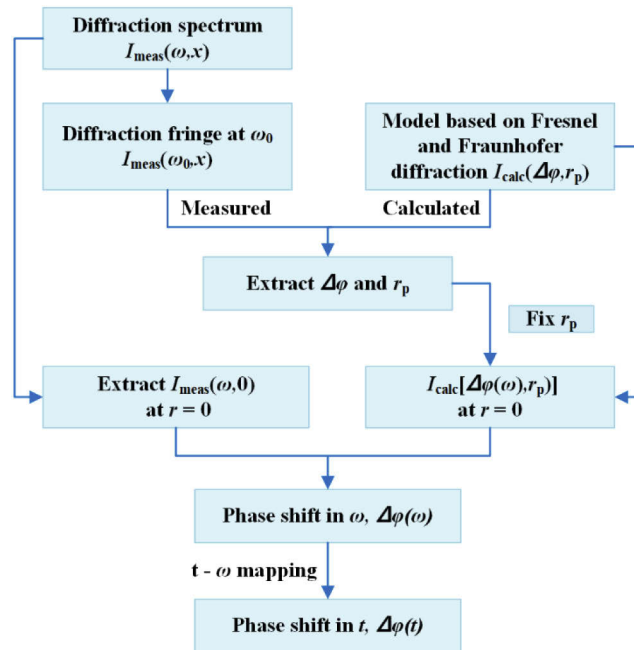


Fig. 2. The calculation flow chart of the proposed method.

Furtherly, the relationship between the average free electron density (N_e) of the plasma column and the phase shift of the probe light can be estimated with the following equation,

$$\Delta\varphi = \frac{2\pi}{\lambda 2N_c} \int_0^{d_p} N_e(z) dz, \quad (4)$$

where the domain of integration $d_p = 2r_p$ is the diameter of the plasma column, which means that the phase shift is the result of the probe light passing through the plasma column with distance of d_p . In the longitudinal diffraction mode [11, 22], the diameter of the plasma column should be replaced by the length of the plasma column. N_c is the critical plasma density, which can be expressed as,

$$N_c = \frac{4\pi^2 c^2 \varepsilon_0 m_e}{e^2 \lambda^2}, \quad (5)$$

where c is the speed of light in vacuum, ε_0 is the dielectric constant, m_e is the mass of the electron, e is the electron charge. According to Eq. (4), the average electron density can be expressed as,

$$N_e = \frac{\lambda N_c \Delta\varphi}{2\pi r_p}, \quad (6)$$

In order to obtain the change of the refractive index Δn in the plasma region, the real part of the refractive index of the plasma can be estimated by the plasma density. The expression can be written as [25],

$$\Delta n \approx -\frac{N_e}{2N_c}, \quad (7)$$

Thus, the dynamics of the probe light phase shift and the corresponding physical parameters of the plasma column within a single-shot measurement can be obtained through a single calculation by the developed method.

3. Results and discussion

3.1. Temporal-spatial diffraction spectrum

The excitation and detection of air ionization is accomplished by the device shown in Fig. 1(a), that is, a femtosecond pulse is used for pumping and a chirped picosecond pulse is used as a probe. The experimental environment is in a thousand-level clean room. The width of the entrance slit of the imaging spectrometer is set as 0.016 mm. Before the measurement, the delay line has been adjusted to ensure that the beginning of air ionization is within the spectrum measurement range. The static (with no pump pulse) and the dynamic (with pump pulse) spectrum recorded on the CCD camera are shown in Fig. 3(a) and (b), respectively. Through differential processing, a 2D diffraction spectrum can be obtained, as shown in Fig. 3(c). The horizontal and vertical axes of the spectrum represent the wavelength dimension and the spatial dimension. It can be observed in the wavelength direction that the spectrum covers the changes before and after the plasma is formed. The demarcation point is at $\lambda = 792$ nm. Figure 3(d) shows the ionization start stage of the spectrum in Fig. 3(c), where the spatial domain has been converted into the actual size and the wavelength dimension has been mapped into the time domain. It should be noted that the moment $t = 0$ in the spectrum is determined by the position where the diffraction fringes appear. The process of the excitation of the gas plasma and its expansion to a quasi-steady state can be demonstrated clearly from the measured spectrum. It takes about 7 ps from the beginning of air ionization to the formation of a quasi-stable plasma column.

3.2. Phase shift extraction

When the probe light passes through the ionization zone, it carries the physical information of the plasma into the CCD detector and generates diffraction fringes. Through the inverse solution

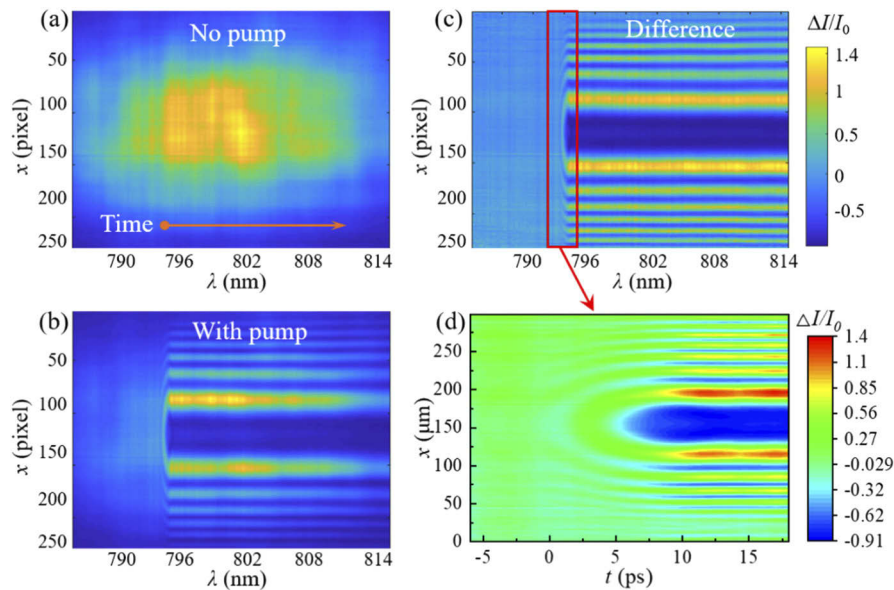


Fig. 3. Spectral images of the probe beam recorded by CCD in the case of (a) without pump pulse and (b) with pump pulse. (c) The difference spectrum of (a) and (b) reflects the onset and the evolution of air ionization. (d) The area in the red box of (c) whose spatial domain has been converted to the actual size and the wavelength has been mapped into the time domain. The pump pulse energy $E_{in} = 1$ mJ.

of the diffraction fringes, some physical parameter changes of the gas in the ionization region can be acquired. Figure 4 shows the measured spatial diffraction fringe (blue balls) extracted from the spectrum at $t = 86$ ps since the ionization started and the corresponding fitting curve (red line) using Eq. (2). It can be seen from the result in Fig. 4 that the fitted curve is in good agreement with the measured data, except for the slight difference in peak values at few locations (such as $r = 60$ μm). These differences may be due to the oscillation in spatial shape of the probe beam, which has negligible influence on the extraction of fitting parameters. As a result, the radius of the plasma column $r_p = 40$ μm and the phase shift $\Delta\varphi = 0.18\pi$ of the probe light induced by the plasma were obtained by the fitting process.

Comparing the diffraction fringes at different times, as shown in Fig. 5(a), it can be found that only the amplitude at the peaks has changed. The peaks on both sides show a slight asymmetry, which may be caused by the deviation of the spectrum. It can be seen that $t = -23$ ps, the spectral line is not a horizontal straight line, but has a slight degree of fluctuation. Here we focus on the change of the central peak of the diffraction fringe, because the prerequisite for deriving Eq. (3) is $r = 0$. Closer inspection of Fig. 5(a) shows that the amplitude of the peak at the central position gradually decreases with time, as shown in Fig. 5(b). Considering that only the phase shift of the probe light is time-varying during this time period. Therefore, the relationship between the peak value at the center of the diffraction fringes and the phase shift is established, as shown in Eq. (3). Under the premise of determining the size of the plasma column, the evolution of the phase shift can be obtained by a single calculation.

As shown in Fig. 6(a), the diameter of the plasma column gradually increases with time in the expansion stage ($0 \sim 7$ ps) of the plasma since the start of the ionization. The size of the plasma is an essential condition for solving the phase shift evolution. The acquired plasma size data were fitted by the Boltzmann function, and the results are shown as the red curve in Fig. 6(a).

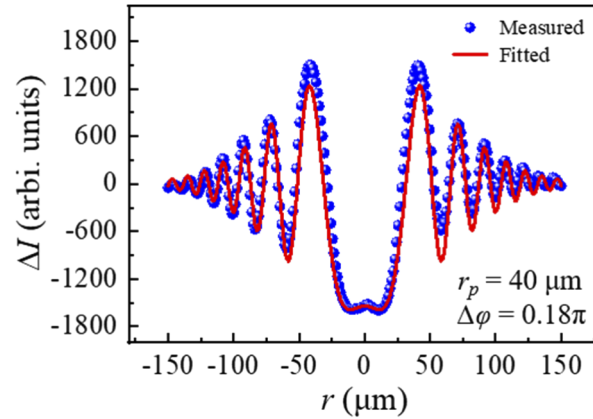


Fig. 4. The diffraction fringe at $t = 86$ ps since the ionization extracted from the measured spectrum (the blue balls) and the fitted curve (red line) obtained by Eq. (2). The fitting results of the parameters (i.e. the plasma radius and the phase shift) are shown in the figure.

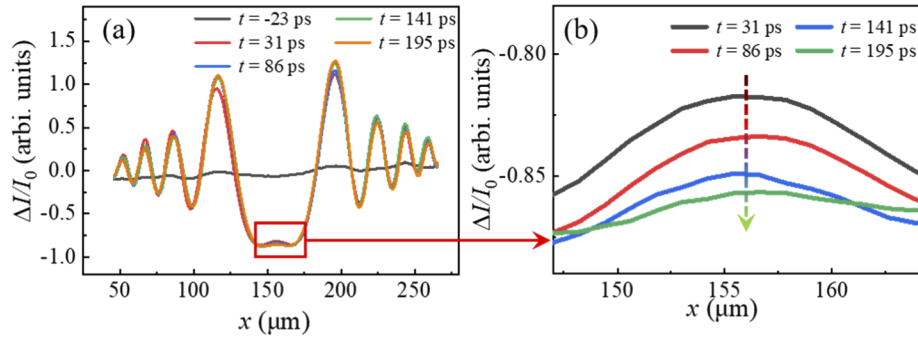


Fig. 5. (a) The spatial distribution of diffraction fringes at different times extracted from the measured spectrum and (b) evolution of the central peak of the fringes. The amplitude of the central peak gradually decreases with time.

Within the stage of $0 \sim 7$ ps, the plasma column diameter gradually increases from 0 to $80 \mu\text{m}$, and then, the plasma column diameter remains at $\sim 80 \mu\text{m}$.

As shown in Fig. 6(b), the black curve depicts the phase shift evolution of the probe light calculated by Eq. (3) i.e. the developed method, the red balls show the results obtained by multiple fitting process using Eq. (2). The consistency of the results proves the correctness and effectiveness of the derived equation and the developed method. From the results, it can be seen that the evolution of the phase shift can be divided into two stages. At first, the phase shift rapidly increases from 0 to 0.62 rad within ~ 7 ps, and then followed by a decrease stage, as shown in the inset of Fig. 6(b), which depicts a slow linear change. It is worth mentioning that the phase change of the probe light is caused by the change of the plasma density in the ionization region. Therefore, the evolution of the phase shift will reflect the evolution of the plasma density.

3.3. Evolution of the average plasma density and the refractive index

The phase shift of the probe light can directly reflect the changes of some physical parameters of the plasma column in the ionization region, such as the average plasma density N_e and the refractive index n . Correspondingly, the relationship between the plasma density and the phase shift was established, as shown in Eq. (4) and Eq. (6). The result of the average plasma

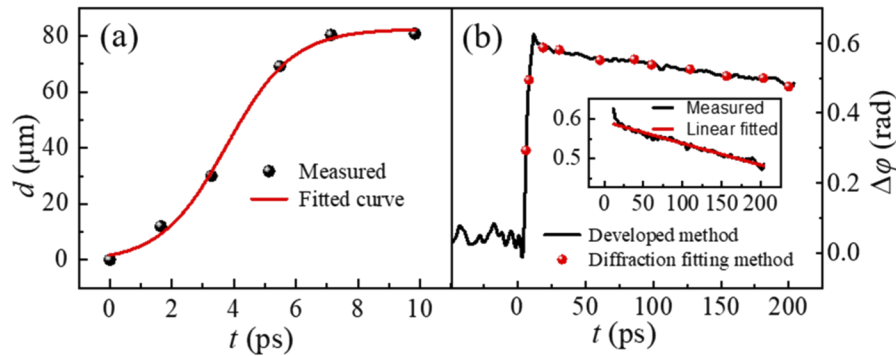


Fig. 6. (a) The diameter of the plasma column extracted from the diffraction fringe at the expansion stage of ionized plasma (black balls) and the Boltzmann function fitting curve; (b) the black curve shows the phase shift evolution calculated by Eq. (3) and the red balls show the results obtained by multiple fitting process using Eq. (2). The inset shows the phase shift evolution at the steady state of the plasma (black line) and the linear fitted curve (red line).

density calculated by Eq. (6) was shown by the black curve in Fig. 7. It can be seen from this plot that the free electron density increases rapidly and reaches the maximum within 7 ~ 8 ps, which is consistent with the results obtained by the interferometry as reported in Ref. [26]. Subsequently, the electron density decreases slowly over a long period of time. The whole evolution process presented here are in good agreement with the numerical results reported by A. Chen *et al.* [30], where the multiphoton ionization process, the avalanche ionization and the electron recombination were considered in the calculation model. The calculation model in [30] can explain the evolution of the plasma density in a consistent manner. When the fs laser pulse is focused in air, the optical breakdown process happens once the intensity exceeds the breakdown threshold [31]. The air molecules in the focal area absorb the laser energy and ionized in the form of multiphoton ionization and avalanche ionization in an ultra-short time to generate a plasma column containing a large number of free electrons, holes and ions. The ionization resulted in a shining light spot and accompanied by a popping sound during the experiment. Then, when the recombination of electrons and holes plays a dominant role, the free electron density no longer increases, but shows a slow decreasing trend.

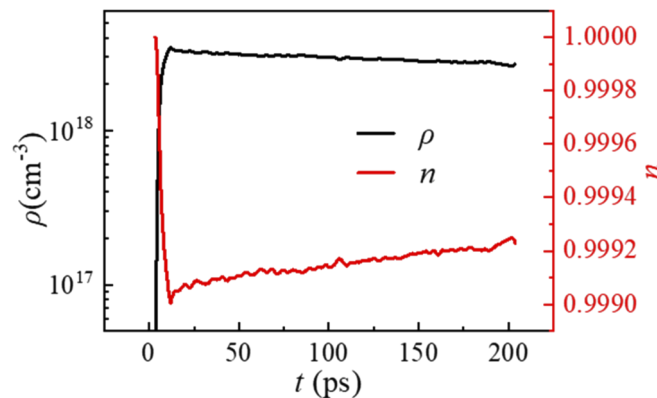


Fig. 7. The calculated free electron density (black) and refractive index evolution (red) by the corresponding models shown in Eq. (6) and Eq. (7), respectively.

The relationship between the free electron density and the refractive index change was shown as Eq. (7). The refractive index evolution profile of the ionization region was shown by the red curve in Fig. 7. The curve exhibits the opposite trend to the electron density changes. The refractive index drops to the minimum of about 0.999 while the electron density reaches its maximum. Then, as the electron density decreases, the refractive index gradually increases. The refractive index of the plasma region is lower than that of air, which can be attributed to the large number of free electrons inside the plasma column [32]. It can be seen from Eq. (7) that the contribution of free electrons to the plasma refractive index is negative, which means that when the number of the free electrons dominates in the plasma, it will lead to $n < 1$, as shown in Fig. 7. And correspondingly, the increase in refractive index is due to the recombination of free electrons.

4. Conclusion

In conclusion, a single-shot diffraction method has been proposed to detect the dynamics of the femtosecond pulse-induced air ionization from the transverse direction. It has been demonstrated that with the configuration proposed in this work, the dynamic evolution of air ionization can be captured in a single measurement, including the formation, expansion and stabilization of the plasma. A sharply increase time of ~ 7 ps of the plasma expansion and a diameter of ~ 80 μm of the plasma column have been depicted in the results with the pump pulse energy of 1 mJ. The temporal profile of the phase shift of the probe light has been extracted by the developed method. Follows the change of phase shift, the evolution of the free electron density and the refractive index of the plasma has been calculated. The proposed method is not only suitable for the dynamic measurement of laser-induced air ionization, but also can be expected to be used for the dynamic detection of the ablated plasma and internal damages in transparent materials.

Funding. National Natural Science Foundation of China (51727809, 51975232); National Key Research and Development Program of China (2017YFF0204705); National Science and Technology Major Project (2017ZX02101006-004).

Acknowledgments. The authors would like to thank the technical support from the Experiment Center for Advanced Manufacturing and Technology in School of Mechanical Science & Engineering of HUST.

Disclosures. The authors declare that there are no conflicts of interest related to this article.

Data availability. Data underlying the results presented in this paper are not publicly available at this time but may be obtained from the authors upon reasonable request.

References

1. A. Couairon and A. Mysyrowicz, "Femtosecond filamentation in transparent media," *Phys. Rep.* **441**(2-4), 47–189 (2007).
2. L. Bergé, S. Skupin, R. Nuter, J. Kasparian, and J.-P. Wolf, "Ultrashort filaments of light in weakly ionized, optically transparent media," *Rep. Prog. Phys.* **70**(10), 1633–1713 (2007).
3. X. C. Zeng, "Simulation and experimental studies on the evolution of a laser spark in air," *Laser Part. Beams* **10**(4), 707–713 (1992).
4. T. X. Phuoc, "An experimental and numerical study of laser-induced spark in air," *Opt. Lasers Eng.* **43**(2), 113–129 (2005).
5. M. Mathuthu, R. M. Raseleka, A. Forbes, and N. West, "Radial Variation of Refractive Index, Plasma Frequency and Phase Velocity in Laser Induced Air Plasma," *IEEE Trans. Plasma Sci.* **34**(6), 2554–2560 (2006).
6. J. Kasparian, M. Rodriguez, G. Méjean, J. Yu, E. Salmon, H. Wille, R. Bourayou, S. Frey, Y. B. André, A. Mysyrowicz, R. Sauerbrey, J.-P. Wolf, and L. L. Wöste, "White-Light Filaments for Atmospheric Analysis," *Science* **301**(5629), 61–64 (2003).
7. X. M. Zhao, J.-C. Diels, C. Y. Wang, and J. M. Elizondo, "Femtosecond Ultraviolet Laser Pulse Induced Lightning Discharges in Gases," *IEEE J. Quantum Electron.* **31**(3), 599–612 (1995).
8. H. Pépin, D. Comtois, F. Vidal, C. Y. Chien, A. Desparois, T. W. Johnston, J. C. Kieffer, B. La Fontaine, F. Martin, F. A. M. Rizk, C. Potvin, P. Couture, H. P. Mercure, A. Bondiou-Clergerie, P. Lalande, and I. Gallimberti, "Triggering and guiding high-voltage large-scale leader discharges with sub-joule ultrashort laser pulses," *Phys. Plasmas* **8**(5), 2532–2539 (2001).

9. R. Ackermann, K. Stelmaszczyk, P. Rohwetter, G. Méjean, E. Salmon, J. Yu, J. Kasparian, G. Méchain, V. Bergmann, S. Schaper, B. Weise, T. Kumm, K. Rethmeier, W. Kalkner, L. Wöste, and J.-P. Wolf, "Triggering and guiding of megavolt discharges by laser-induced filaments under rain conditions," *Appl. Phys. Lett.* **85**(23), 5781–5783 (2004).
10. T. X. Phuoc, "Laser-induced spark ignition fundamental and applications," *Opt. Lasers Eng.* **44**(5), 351–397 (2006).
11. F. Théberge, W. W. Liu, P. T. Simard, A. Becker, and S. L. Chin, "Plasma density inside a femtosecond laser filament in air: strong dependence on external focusing," *Phys. Rev. E* **74**(3), 036406 (2006).
12. S. Bodrov, V. Bukin, M. Tsarev, A. Murzanev, S. Garnov, N. Aleksandrov, and A. Stepanov, "Plasma filament investigation by transverse optical interferometry and terahertz scattering," *Opt. Express* **19**(7), 6829–6835 (2011).
13. Y. Liu, T. Wang, N. Chen, S. Du, J. Ju, H. Sun, C. Wang, J. Liu, H. Lu, S. L. Chin, R. Li, Z. Xu, and Z. Wang, "Probing the effective length of plasma inside a filament," *Opt. Express* **25**(10), 11078–11087 (2017).
14. W. Liu, Q. Luo, and S. L. Chin, "Competition between multiphoton/tunnel ionization and filamentation induced by powerful femtosecond laser pulses in air," *Chin. Opt. Lett.* **1**(1), 56–59 (2003).
15. H. Schillinger and R. Sauerbrey, "Electrical conductivity of long plasma channels in air generated by self-guided femtosecond laser pulses," *Appl. Phys. B: Lasers Opt.* **68**(4), 753–756 (1999).
16. S. Tzortzakis, B. Prade, M. Franco, and A. Mysyrowicz, "Time-evolution of the plasma channel at the trail of a self-guided IR femtosecond laser pulse in air," *Opt. Commun.* **181**(1-3), 123–127 (2000).
17. A. Ting, I. Alexeev, D. Gordon, R. Fischer, D. Kaganovich, T. Jones, E. Briscoe, J. Peñano, R. Hubbard, and P. Sprangle, "Measurements of intense femtosecond laser pulse propagation in air," *Phys. Plasmas* **12**(5), 056705 (2005).
18. H. Yang, J. Zhang, Y. Li, J. Zhang, Y. Li, Z. Chen, H. Teng, Z. Wei, and Z. Sheng, "Characteristics of self-guided laser plasma channels generated by femtosecond laser pulses in air," *Phys. Rev. E Stat. Nonlin. Soft Matter Phys.* **66**(1), 016406 (2002).
19. V. V. Bukin, N. S. Vorob'ev, S. V. Garnov, V. I. Konov, V. I. Lozovoi, A. A. Malyutin, M. Ya. Shchelev, and I. S. Yatskovskii, "Formation and development dynamics of femtosecond laser microplasma in gases," *Quantum Electron.* **36**(7), 638–645 (2006).
20. X. L. Liu, X. Lu, X. Liu, T. T. Xi, F. Liu, J. L. Ma, and J. Zhang, "Tightly focused femtosecond laser pulse in air from filamentation to breakdown," *Opt. Express* **18**(25), 26007–26017 (2010).
21. P. Chizhov, V. Bukin, and S. Garnov, "Interferometry in Femtosecond Laser Plasma Diagnostics," *Phys. Procedia* **71**, 222–226 (2015).
22. J. Liu, Z. Duan, Z. Zeng, X. Xie, Y. Deng, R. Li, Z. Xu, and S. L. Chin, "Time-resolved investigation of low-density plasma channels produced by a kilohertz femtosecond laser in air," *Phys. Rev. E Stat. Nonlin. Soft Matter Phys.* **72**(2), 026412 (2005).
23. J. Liu, Z. Duan, Z. Zeng, X. Xie, Y. Deng, R. Li, and Z. Xu, "Transverse evolution of a plasma channel in air induced by a femtosecond laser," *Opt. Lett.* **31**(4), 546–548 (2006).
24. G. Rodriguez, A. R. Valenzuela, B. Yellampalle, M. J. Schmitt, and K.-Y. Kim, "In-line holographic imaging and electron density extraction of ultrafast ionized air filaments," *J. Opt. Soc. Am. B* **25**(12), 1988–1997 (2008).
25. Z. Sun, J. Chen, and W. Rudolph, "Determination of the transient electron temperature in a femtosecond-laser-induced air plasma filament," *Phys. Rev. E Stat. Nonlin. Soft Matter Phys.* **83**(4), 046408 (2011).
26. C. Y. Chien, B. La Fontaine, A. Desparois, Z. Jiang, T. W. Johnston, J. C. Kieffer, H. Pépin, and F. Vidal, "Single-shot chirped-pulse spectral interferometry used to measure the femtosecond ionization dynamics of air," *Opt. Lett.* **25**(8), 578–580 (2000).
27. K. Y. Kim, I. Alexeev, and H. M. Milchberg, "Single-shot measurement of laser-induced double step ionization of helium," *Opt. Express* **10**(26), 1563–1572 (2002).
28. Y.-H. Chen, S. Varma, I. Alexeev, and H. M. Milchberg, "Measurement of transient nonlinear refractive index in gases using xenon supercontinuum single-shot spectral interferometry," *Opt. Express* **15**(12), 7458–7467 (2007).
29. Z. Zhong, W. Gong, H. Jiang, H. Gu, X. Chen, and S. Liu, "Investigation of Spatial Chirp Induced by Misalignments in a Parallel Grating Pair Pulse Stretcher," *Appl. Sci.* **10**(5), 1584 (2020).
30. A. Chen, S. Li, S. Li, Y. Jiang, J. Shao, T. Wang, X. Huang, M. Jin, and D. Ding, "Optimally enhanced optical emission in laser-induced air plasma by femtosecond double-pulse," *Phys. Plasmas* **20**(10), 103110 (2013).
31. P. Polynkin and J. V. Moloney, "Optical breakdown of air triggered by femtosecond laser filaments," *Appl. Phys. Lett.* **99**(15), 151103 (2011).
32. D. Breitling, H. Schittenhelm, P. Berger, F. Dausinger, and H. Hügel, "Shadowgraphic and interferometric investigations on Nd: YAG laser-induced vapor/plasma plumes for different processing wavelengths," *Appl. Phys. A: Mater. Sci. Process.* **69**(7), S505–S508 (1999).